Insights on performance and an improved model for full scale electrolysers based on plant data for design and operation of hydrogen production

Insights on Performance and an Improved Model for Full Scale Electrolysers based on Plant Data for Design and Operation of Hydrogen Production

Maja Persson[1], Dimitri Mignard[1*], David Hogg[2]

1. University of Edinburgh, School of Engineering, Institute of Energy Systems
2. Bright Green Hydrogen, The Business Partnership Ltd

* Corresponding author

Abstract: Developers and operators of energy systems based on renewable energy require effective models of these systems, including those with hydrogen storage where electrolysers are critical components. However, electrolyser models are often either too detailed to be computationally-efficient within whole system model, or too inaccurate at times of low production of renewable energy. Our novel model addresses this by combining the Tafel equation and an original model for Faradaic efficiency. It was validated and tested on plant data from the 250 kW electrolyser at Bright Green Hydrogen's Levenmouth Community Energy Project in Methil, Scotland. The model estimated hydrogen consumption more accurately than the 'Linear Model' habitually used in industry. Our data also emphasized the importance of an optimised control scheme for minimizing hot standby losses. Pressurisation during start-up, purging and pressure-driven fluctuations also contributed significant losses and scatter when inspecting minute-by-minute data. This knowledge should inform whole system analysis and control.

1. Introduction

1.1. Background

The interest in hydrogen as an energy vector is growing worldwide. Hydrogen brings to energy systems its versatility of applications, as well as the ability to provide energy storage at relatively high density, at scale and for longer periods than other means such as batteries. The UK is currently working on a possible future hydrogen economy, with for example the production of three white papers in 2017 by the H2FC consortium that analysed the role of hydrogen in energy security, future energy systems and its economic impacts [1]–[3]. Furthermore, the European Commission has recognised hydrogen from renewable energy as a necessity and priority for reaching the EU's climate neutrality and zero pollution goal, setting itself a target to install at least 6 GW of renewable hydrogen electrolyser capacity between 2020 and 2024, and 40 GW between 2025 and 2030 [4]. This is intended as the basis for an industry that will supply a wide range of needs such as hydrogen refuelling stations, trucks, rail, maritime and energy storage. The Committee on Climate Change published a report in 2019 on how UK can reach net-zero in emissions by 2050, where hydrogen was highlighted multiple times as a possible solution, especially for sectors that are difficult to decarbonise for example HGVs and ships [5].

Meanwhile, the energy system in Scotland illustrates well the challenges and opportunities for energy storage and hydrogen. In 2018 around 26,500 GWh of renewable energy provided nearly 74% of the demand for electrical energy [6]. At times, some of this energy is in excess of local demand and must be exported if possible, but curtailment of some of this excess due to network congestion is responsible for the loss of around 16% of Scotland's onshore wind energy [7]. A recent report investigated the use of this curtailed power for hydrogen production by electrolysis, and found that curtailment levels of 15-25% would suffice for the economic viability of this scheme [8]. While non-curtailed power would be more profitable for electrolysis plants in the current context (especially due to the fact that it is more continuously available and allow a greater utilization capacity of the assets), this gap is expected to close in the context of fast growing wind capacity. The ScotWind offshore wind leasing round on its own will increase rated generating capacity by up to 10 GW [9], [10].

However, electricity represents only 24% of Scottish energy demand, with 51% of this demand coming from water- and space heating and 25% for transport [11]. Therefore, the scope for utilising this excess renewable power for decarbonising heat and transport is significant. For example, the UK published a Clean Growth Strategy report in 2017, highlighting that transport alone was the cause of 24% of UK's emissions in 2015 [12]. In Scotland, internal transport (excluding international aviation and shipping) accounted for 32.1% of the total greenhouse gases emissions in 2017 [13].

In this context, energy storage technologies with multiple possible uses would be advantageous, making hydrogen a strong contender given its ability to provide electricity, heat and vehicle fuel on demand and with minimal emissions [14]. The prospect of improving energy security (including for remote communities) and getting more value from renewable energy has motivated the Scottish Government's commitment to work with industry and academia to further develop the role of hydrogen in the energy system, as stated in its Energy Strategy [11].

A wide range of published studies on electrolytic hydrogen already exists. For example, some of these studies compared business cases for storing or utilising the power output from offshore windfarms [15]; others modelled wind energy with hydrogen storage with the goal of meeting 100% of the demand [16]. Hydrogen also compares very favourably against other storage technologies when considering long term storage [17], and is therefore an option for seasonal energy storage. For example, a study on Mykines, Faroe Islands, compared it to the existing diesel generators to help with the seasonal tourism. The high energy demand from tourism did not match the time periods of peak output from the installed wind energy. Although hydrogen was more expensive, it still had a strong case when comparing its environmental impact to the diesel generator as well as optimising the energy generated from the existing wind turbines [18]. The consideration of environmental impact helping hydrogen's case when compared to traditional plant solutions was also highlighted in a hydrogen seasonal storage simulation done in northern Italy [19]. Island communities have resulted in several energy systems studies due to factors such as fuel import dependency [20], high local renewable energy sources with exporting challenges [21], [22] and high energy costs [23], [24]. A study looking at comparing hydrogen and electric ferries for zero emission ferry lines between Croatian Islands using 100% renewable energy found that the best of the two technologies varied on island size and route, but that overall there was a struggle to both keep the electricity export/import at equilibrium and locally supply enough electricity for the ferry lines [20]. A paper summarising the demonstration PURE project in Unst, Shetland Islands, found that connecting an electrolyser with 3.55 Nm^3/hour maximum hydrogen output and a 5 kW fuel cell to two 15 kW wind turbines meant that 18% more of the total wind energy was captured [24]. The project also resulted in an additional income generated for local businesses and therefore helped the community. Furthermore, several studies on the storage of hydrogen for seasonal fluctuations suggest underground storage as a better alternative, for example salt caverns and (for weeks-worth of storage) depleted natural gas reservoirs, due to the available space at the required scale [25]–[29]. This ability to provide seasonal storage may contribute to justify the deployment of a wider infrastructure for the transmission and distribution of hydrogen, within which smaller scale systems may be present.

Flagship demonstration projects are currently taking place to initiate and validate the deployment of hydrogen technologies in Scotland. We will briefly mention the Aberdeen hydrogen buses, and the activities in Orkney, both relying on the production of hydrogen by electrolysis of water using renewable power.

Aberdeen has been leading the way in demonstrating how a city can reduce its emissions through the hydrogen bus project [30], funded by two separate European projects, High Vlo City and HyTransit, both supported by Fuel Cells and Hydrogen Joint Undertaking (FCHJR). Since then, the city has opened a hydrogen re-fuelling station at the end of 2018 [31], supporting the existing 37 hydrogen vehicles in the city as well as meeting planned future demand, including 10 new hydrogen buses expected at the end of 2019.

Meanwhile in the Orkney Islands, demonstration projects have been underway to address the current over-production of renewable energy relative to the island population and network constraints. In particular, power production often exceeds the rated capacity of power cables, including between islands, and between the archipelago and the mainland [32]. Local communities are experiencing loss of revenue due to enforced curtailment (i.e. dumping) of power produced. The Surf 'n' Turf project focused on one of the islands, Eday, which hosts a population of 150 people, as well as a 900 kW community wind turbine that was vulnerable to curtailment and the tidal energy test site of the European Marine Energy Centre (EMEC) [32]. The project has been producing hydrogen on the island, then shipped by ferry to Kirkwall (the Orkney Islands capital on the archipelago 'mainland'), where the hydrogen is converted back to electricity and used on demand for 'cold ironing' of the ferries (i.e. the supply of power to ships that are anchored in docks), thus cutting back on pollution

from diesel fumes in the port area [32]. The Surf 'n' Turf project is the world's first to produce hydrogen from tidal power [21], [32]. The BIG HIT project builds on Surf 'n' Turf, as it includes the island Shapinsay with its 900 kW wind turbine, bigger capacity of hydrogen production, a hydrogen boiler on the same island and more varied hydrogen use at Kirkwall including using the hydrogen to power part of the harbour buildings, 3 ferries and 5 hydrogen fuel cell vehicles [22]. Other hydrogen projects in Orkney include: HySpirits investigating using hydrogen to operate a thermal fluid system instead of combustion fuel within the distilling industry; HyFlyer looking at a demonstration flight using hydrogen fuel cell powertrain for 250-300 nautical miles long flights; and HyDime project investigating hydrogen/diesel dual fuel commercial ferries [21].

Finally, the Levenmouth Community Energy Project ran in Methil (Scotland) in 2016-17, and since that project provided the direct background and the data for this paper, we are covering it in more detail in the next section. All together, these projects show how electrolytic hydrogen might be part of the energy storage solution, by also providing transport and heat rather than just storing electrical energy.

1.2. The Levenmouth Community Energy Project

The Levenmouth Community Energy Project (LCEP) was created and launched in 2014 by Bright Green Hydrogen (BGH), a not-for-profit company based in Methil, Scotland. Prior to that, BGH had successfully completed The Hydrogen Office Project (THO), where the excess energy from a 750 kW wind turbine was stored as hydrogen as a backup for providing low carbon power to an office building via a fuel cell [33]. The project's main goal was to encourage de-carbonising energy supplies and its findings fed into further research on electrolytic hydrogen [34].

The LCEP was an expanded project from THO, taking the concept further. In addition to the 750 kW wind turbine, the renewable generators that fed into the system also included:

- 48kW of roof-mounted PV and 112 kW of ground PV, securing a varied mix of energy sources that could at times complement each other or ensure a more continuous supply.
- A 250 kW PEM electrolyser;
- 45 kg of hydrogen storage at 30 bar, equating to roughly 1425 kWh of energy storage (at Lower Heating Value);
- A 100 kW fuel cell;
- Two 60 kW hydrogen refuellers, one PEM and one alkaline;
- A total of 17 hydrogen vehicles of three different models: 10 Renault Kangoo Electric Vehicles with fuel cells, 5 Diesel-Hydrogen Ford Transits and 2 Diesel-Hydrogen Refuse Collection Vehicles.

BGH aims to show the potential of hydrogen through practical demonstrations, collecting data for further learning. This information enables the modelling and exploring of hydrogen systems using real-world data.

The present paper focuses on using that data to develop an electrolyser model derived in part from previous work [35], but with amendments to take advantage of the "real-life" nature of the data allowing for a more accurate representation of full-scale systems. The model is also adapted so as to make good use of the limited amount of data available due to instrumentation and proprietary restrictions on data, as can happen in the commercial setting, as an improvement on the existing models.

1.3. Existing models of electrolysers

The electrolyser plays a crucial part when modelling a hydrogen system, and for that purpose a number of electrolyser models are presented in the literature. Most of these models proceed from the basic set of equations linking the applied potential to the current and hydrogen production in an electrolysis cell [36], [37], and each is adapted according to its application or the background of the authors. The degree of detail and complexity of these models vary widely, as mentioned in [38], from simple linear models that link the hydrogen production to the power input, to more detailed electro-chemical models. The more detailed models have different areas of focus, ranging from investigating effects of cell voltage and internal components [39], [40], to separate material balances

for each electrode [41]; to detailed deterministic electrical, electrochemical, ionic transport and thermodynamic behaviour [37], [42]–[45]. Some focus on capturing the main behaviour observed using empirical models [46][47].

Although they all have their uses, models of the type encountered in [35], [39], [41], [42], [48] have a level of complexity that may be too high for using in full scale hydrogen energy systems modelling as it would affect the overall system computational efficiency, and parameters may be required that are often difficult to get for commercial electrolysers. Some of models have highlighted the importance when considering the electrolyser system to not just evaluate the behaviour of the stack, but include the balance of plant components such as pump, cooling unit and converters [49], [50].

Of the simpler models that have been applied to demonstration scale systems, the Ulleberg model [51] is a well-known and tested semi-empirical model and several studies have used it or based new models from it [42], [43], [47], [52], [53]. However, many parameters are still difficult to estimate and their values must be adjusted by trial and error without much knowledge of whether they represent real physical data or just convenient fits [51]. The alternative is a simple linear model [46], evaluated in [38], in which a commercial electrolyser performance is described by a linear polarisation curve, i.e. a linear relationship between the voltage and the current applied to individual electrolysis cells (the "polarisation curve"). This type of model is straightforward to incorporate into an energy system with very few inputs needed. However, it may be asked whether it captures enough accuracy for a user given that in our experience it does not capture energy consumption well at low load. We also learnt from this project and others that the energy consumption during stand-by mode (when the electrolyser is inactive but maintained in a state of readiness to operate at short notice) can be significant, an aspect which requires consideration of the control of operation and possibly the power supply too when modelling the electrolyser as part of a wider energy system.

Ideally, a dynamic model that described the operation of an electrolyser stack would represent the fundamental mechanisms at play in a simple but realistic manner. This model would include a small number of parameters that could be adjusted to fit the model to limited plant data available to the operators. The fitted values of these parameters in the model would be within an expected range based on known physical properties of materials, likely dimensions of internal components when not known and coefficients based on fundamental physical models. We developed one such model based on real-life installation as described in the next section. We also reported our observations on the parasitic losses during stand-by operation, which we will incorporate in a model of the wider LCEP system to be presented in a forthcoming paper.

2. The Electrolyser Model

2.1 Available Data

The usable plant data for the 250 kW PEM electrolyser that was available to the operator (BGH) was limited to time series of paired energy usage of the stack of cells, $P_{measured,}$ and corresponding hydrogen produced n_{H2}.

Several existing models e.g. [47], [51], [54] include temperature effects, however, the temperature data available at BGH was not sufficient for inclusion in this study.

Furthermore, the following information was known from the product specifications and personal communication with the site's hydrogen system contractor:

- Maximum power capacity P_{rated} , 250 kW
- Maximum current I_{rated}, 3050 A
- Maximum DC voltage, U_{rated}, 85 V
- Max volumetric flowrate $n_{H2,max}$ of hydrogen produced, 45 Nm^3/hr or 3.78 (H_2)kg/hr
- Number of stacks, 1
- Surface area of individual cells, 1500 cm^2

The data for volume of the hydrogen produced was measured by a Bronkhorst In-Flow F-113AI and reported in Nm^3/hr, Nm^3 being m^3 at normal conditions of pressure and temperature (1 atm and 20 ^oC).

The overall set of data from the LCEP was subdivided into two subsets, one for the development of the model and one for its validation.

2.2 Assumptions and Limitations

To complete the model, certain assumptions were established:

1. The maximum rated power capacity (250 kW) includes the powering of not just the stack (or stacks) of electrolytic cells, but also the balance of whole electrolyser (pumps, cooling fans, controls), and it also includes a proportion of loss from the receiving transformer and from the rectifier that feeds DC to the stack. Plant data suggests that at maximum hydrogen production, the measured power going to the stack is $P_{measured,max}$ ~ 176 kW. It was therefore assumed that there were some losses involved between the total power going to the electrolyser (as supplied as a packaged, self-contained plant by the manufacturer) and where the measurement was made. Furthermore, the actual current and voltages corresponding to I_{rated} and U_{rated} were not made available to the operator, so the equations will be in terms of Faradaic current equivalent to the specific hydrogen production.
2. While hydrogen flow data was reported at normal operating conditions of temperature (293K) and pressure (1 atm), the electrolyser maximum allowable working pressure was quoted as 40 bar, suggesting an operating pressure in the region of 30 bar (this is common practice for saving on compression costs downstream of the electrolyser). This pressurisation was assumed not to significantly affect the efficiency of the stack itself [55].
3. A previous study suggested that assuming a constant and nominal operating temperature for the modelling would only over-estimate hydrogen production by 3% [53]. Therefore, it was decided to use normal temperature in this work, although temperature effects could be considered again later in the context of modelling the dynamics of cold start when the electrolyser requires initial warming up.

2.1. Basic Equations for the Power Model

The starting point of our model is the relationship between the potential applied across an electrolysis cell, U_{cell}, and the current in the cell that takes part in the reaction ([32], [33]).

If doing so, the current to be used is $I_{H2,\ cell}$, which is the Faradaic current equivalent to the specific hydrogen production. It is equal to the current going to the cell, I_{cell}, corrected for by the Faraday efficiency, η_F:

$$I_{H2,\ cell} = \eta_F \cdot I_{cell} \quad (1)$$

The Nernst equation detemines a reversible potential for the reaction, U_{rev}, taken here as 1.23 V at 25°C and 1 atm [48], [56]. When a current is fed to the cell, U_{rev} is then augmented by two contributions: Firstly, the internal resistance of the cell, R_{cell}, which simpy increases linearly with $I_{H2,\ cell}$; and secondly, the Tafel equation which gives a logarithmic dependency on $I_{H2,\ cell}$ [57]:

$$U_{cell} = U_{rev} + R_{cell} I_{H2\ cell} + k \ln(I_{H2\ cell}) - k \ln(I_0) \quad (2)$$

Where

I_o is the "exchange current" when no net reaction is taking place (at the equilibrium potential) ;

k is a constant and defined by:

$$k = \frac{R_{gas} T}{0.25 z F}$$

in which R_{gas} is the ideal gas constant (8.314 J K^{-1} mol^{-1}), T is the temperature in K, z is 2 for hydrogen and F is Faraday's constant (96,485 C s^{-1}).

The exchange current is not known, so in order to eliminate this one variable, we rearrange Equation 2 when applied to the known maximum rated hydrogen production,

$$k\ln(I_0) = U_{rev} - U_{H2\ cell,max} + R_{cell}I_{H2\ cell,max} + k\ln\left(I_{H2\ cell,max}\right) \quad (3)$$

Here we have approximated the Faraday efficiency to a value of 1, which is a valid assumption at maximum load and sufficient for our purpose as it is often assumed to be more than 99% [41], [47]. Combining equations (2) and (3) to eliminate I_o:

$$U_{cell} = U_{rev} + R_{cell} * I_{H2\ cell} + k\ln(I_{H2\ cell}) - [U_{\ rev} - U_{H2\ cell,max} + R_{cell}I_{cell,max} + k\ln\left(I_{H2\ cell,max}\right)] \quad (4)$$

The plant data readily available to Bright Green Hydrogen did not include the cell voltage of the electrolyser, but did have the power consumption. Multiplying both sides of equation (4) with the current, $I_{cell,}$ enabled this data to be used since $P_{cell} = U_{cell}I_{cell}$. On the left hand side, the power data appears, while on the right hand side, introducing the Faraday's efficiency allows retaining $I_{H2,\ cell}$ as the sole variable, which itself is directly linked to the hydrogen production rate n_{H2} (in mol/s) through Faraday's law:

Equation (4) could therefore be re-written as:

$$P_{cell} = U_{cell}I_{cell} = \frac{I_{H2\ cell}}{\eta_F}\left[U_{H2\ cell,max} + R_{cell}(I_{H2\ cell} - I_{H2\ cell,max}) + k\ln\left(\frac{I_{H2\ cell}}{I_{H2\ cell,max}}\right)\right] \quad (5)$$

With $I_{H2,stack} = zF \cdot n_{H2}$ (6),

which was also applied to determine $I_{H2\ stack,max}$ at maximum hydrogen flow rate.

Switching to the whole stack of cells, we consider the number of cells n_c.

In Equation (5),

$\ln\left(\frac{I_{H2\ cell}}{I_{H2cell,max}}\right)$ is the same as $\ln\left(\frac{I_{H2\ stack}}{I_{H2stack,max}}\right)$, since $\ln\left(\frac{I_{H2\ cell}}{I_{cell,max}}\right) = \ln\left(\frac{\frac{I_{H2\ stack}}{n_c}}{\frac{I_{H2stack,max}}{n_c}}\right)$.

Also, $R_{cell}\left(I_{H2\ cell} - I_{H2\ cell,max}\right)$ can be re-written as $R_{cell}(\frac{I_{H2\ stack} - I_{H2stack,max}}{n_c})$.

After multiplying on both sides by n_c, Equation (5) therefore becomes:

$$P_{stack} = n_c * P_{cell} = \frac{I_{H2\ stack}}{\eta_F}\left[U_{H2\ cell,max} + \frac{R_{cell}}{n_c}(I_{H2\ stack} - I_{H2\ stack,max}) + k\ln\left(\frac{I_{H2\ stack}}{I_{H2\ stack,max}}\right)\right] \quad (7)$$

Equation (7) gives the power consumption of the stack as a function of the Faradaic current $I_{H2\ stack}$ equivalent to the specified hydrogen production. Parameters are η_F, $U_{H2\ cell,max}$, $\frac{R_{cell}}{n_c}$ and $I_{H2\ stack,\ max}$.

- η_F is initially assumed to have a value of 1, which is reasonably expected to be the case at high load.
- $I_{H2\ stack,\ max}$ is estimated from applying Faraday's law to the maximum rated hydrogen production at η_F = 1. It may correspond to a combined total of Faradaic currents rather than an actual current seen anywhere in the stack.
- $U_{H2\ cell,max}$ can be estimated from the observed power draw at the maximum rated hydrogen production and $I_{H2\ stack,\ max}$.

- $\frac{R_{cell}}{n_c}$ must be adjusted so that the model fits the observed data.

The power fed to the 250kW electrolysis plant is not just feeding into the stack. The electrolyser also includes power consuming components such as a transformer and rectifier and balance of plant (pumps, fans, controls). There are therefore losses involved before the power reaches the electrolyser stack, for example the rectifier, which was investigated during a previous electrical analysis study on the site [58]. When looking at the data available at BGH, it was assumed that the measured power data includes a conversion loss, η_{conv}, in other words:

$$P_{measured,max} = \eta_{conv} * P_{rated} = \eta_{conv} * U_{rated} * I_{rated} \quad (8)$$

An electrolyser can either be in monopolar of bipolar configuration [51], [56]. For monopolar configuration, the stack voltage is the same as cell voltage, $U_{H2\ cell} = U_{H2\ stack}$. Individual electric currents fed to the cell add up to the total electric current fed to the stack (the cells are connected in parallel). The faradaic currents $I_{H2\ cell}$ and $I_{H2\ stack}$ mirror this relationship, $n_c * I_{H2\ cell} = I_{H2\ stack}$.

Meanwhile, for bipolar configuration the overall stack voltage is applied across the cells arranged in series, hence $n_c * U_{H2\ cell} = U_{H2\ stack}$. Also, as a result of this the value for the electric current fed to each cell is the same as the total current fed to the stack. However, the total number of electrons transferred to hydrogen still multiplies with the number of cells, hence the relationship for the combined total of Faradaic currents is the same as for monopolar configuration, $n_c * I_{H2\ cell} = I_{H2\ stack}$.

Therefore, $n_c * I_{H2\ cell} = I_{H2\ stack}$ applies *irrespective* of monopolar or bipolar configuration, and hence $U_{H2\ cell,max}$ is:

$$U_{H2\ cell,max} = \frac{\eta_{conv} * P_{rated}}{n_c * I_{H2\ cell,max}} = \frac{\eta_{conv} * P_{rated}}{I_{H2\ stack,max}} \quad (9)$$

Finally, this led to an equation that models the power going to the electrolyser stack. The stack power is now named P_{model} and is the predicted power attempted to fit the data from the measured power $P_{measured}$. For simplification, the term $\frac{R_{cell}}{n_c}$ from equation (7) has been labelled R and is a resistance parameter:

$$P_{model} = \frac{I_{H2}}{\eta_F}\left[U_{max,cell} + R * [\![(I]\!]_{H2} - I_{max,stack}) + k \cdot \ln\left(\frac{I_{H2}}{I_{max,stack}}\right)\right] \quad (10)$$

At high load, near the maximum power, where it can be assumed that the value for η_F is close to 1, equation (10) simplifies to

$$P^* = I_{H2} * \left[U_{max,cell} + R * [\![(I]\!]_{H2} - I_{max,stack}) + k \cdot \ln\left(\frac{I_{H2}}{I_{max,stack}}\right)\right] \quad (11)$$

where P^* is an approximation of P_{model} at high load. If taking an arbitrary value of η_{conv} in the expected range, for example 0.74, the value of R can be adjusted so that equation (11) can match the observed data for high hydrogen flow rates on a plot of P *vs.* n_{H2}.

Although the Faraday's efficiency was assumed to be equal to or approaching 1 at higher hydrogen production rates, it will be increasing from 0 at the lower rates [59]. This is because at voltages close to the minimum that is required for electrolysis, the leakage currents through the stack can be of an order of magnitude that is greater than that of the current going to react at the electrodes.

At low load, the observed value of η_F must be estimated from the plant data. Noting that formally:

$$\eta_F = P^* / P_{model} \quad (12)$$

we can use equation (12) to get an approximation for the measured value of η_F if using the measured power $P_{measured}$ as an estimate for P_{model}, together with the calculated value of P^* as given by equation (11). For clarity, a different notation can be introduced:

$$\eta_{F,est} = P^* / P_{measured} \quad (13)$$

To model the changing faradaic efficiency, the electrons going to the cells were considered to be either leaking through to the opposite electrode (leakage current), or contributing to producing hydrogen. Hence,

$$\eta_F = \frac{I_{H2} - I_{H2,reverse}}{I_{H2} + leakage\ current} \quad (14)$$

Where $I_{H2,reverse}$ is the reverse current from hydrogen recombining with oxygen species to produce water, and I_{H2} is the forward current actually going to hydrogen production.

$I_{H2,reverse}$ was considered to be approximately equal to the exchange current I_0 at the reversible voltage U_{rev} (1.23 V) when the electrolysis half-cell reactions at the electrode match their respective reverse reaction. This value decreases and very rapidly becomes negligible before I_{H2} as the applied voltage rises above the equilibrium voltage, and therefore the following approximation is acceptable:

$$\eta_F = \frac{I_{H2} - I_0}{I_{H2} + leakage\ current} \quad (15)$$

At the reversible potential (U_{rev} = 1.23 V), $I_{H2} = I_0$. At this point, Faraday's efficiency will be equal to 0, consistent with our expectation.

All terms in equation (15) were then divided by the exchange current, I_0. If we apply Tafel's law to the current ratio I_{H2} / I_o, we can then express η_F as a function of the stack overpotential, itself the difference between U_{stack} and the sum of U_{rev} and the activation potentials at the electrodes, ΔU_{act}. The later quantity will need adjusting for the model to fit $\eta_{F,est}$ from plant data, but is expected to be in the range 0.1 – 0.2 V [13]. The leakage current is expected to simply follow Ohm's law, producing a term that is proportional to U_{stack}. The resulting model for η_F is

$$\eta_F = 0.97 * \frac{Exp(x_1 * (U_{stack} - U_{rev} - \Delta U_{act})) - 1}{Exp(x_1 * (U_{stack} - U_{rev} - \Delta U_{act})) + x_2 * U_{stack}} \quad (16)$$

where x_1 and x_2 are adjustable parameters that can be set to match $\eta_{F,est}$ from plant data, and a factor of 0.97 is introduced to give a more realistic value of η_F at full load rather than 1. U_{stack} itself is obtained with help from equation (6) and (13). The very characteristic shape of the curve for $\eta_{F,est}$ plotted against U_{stack} (as shown in the next section) made the adjustment of ΔU_{act}, x_1 and x_2 fairly straightforward.

2.3 Parameter fitting to match plant data

It is clear from the equations in section 2.2, that the model requires data-fitting methods. Finding the unknown parameters for this model was done heuristically by visual fitting of modelled curves to scatter plots of minute-by-minute experimental data that were obtained for the electrolyser on a specific day, June 1st, 2017, for the whole day. These adjustments were made by implementing the model in an Excel spreadsheet, and assuming reasonable starting values for the parameters. The results of the model were plotted on the same graph as the plant data and the values of the parameters were then adjusted so that the model curve matched the data, as described in the rest

of this section. This approach avoids the use of complex optimization methods. Exploring the sensitivity of the fit of the model to changes in value of individual parameters confirmed that the proposed solution was an approximation of a local optimum, acceptable for our purpose. Therefore, we deemed our approach to be practical enough for end-users who have sufficient knowledge of electrolyser behaviour, as long as the data is of good enough quality to clearly denote expected trends.

First, we concentrate on the experimental data at high load. The nominal rating for hydrogen production at maximum load for the electrolyser (3.78 kg/hr, or 1.05 g/s) is reached during operation as seen in the experimental data (Figure 2). The corresponding measured power $P_{measured}$ is approximately in the range 175 – 200 kW. Given the rating for the full electrolyser system (250 kW), this suggests a value for the conversion efficiency factor value from power supply to stack (η_{conv}) that lies between 175/250 = 0.7 and 200/250 = 0.8. A tentative value must be chosen in this range before proceeding. We arbitrarily set η_{conv} = 0.74 and found this value to be a good enough choice for the rest of the modelling effort on this system.

Still considering the power at high load, we assume a Faraday's efficiency of 1, P^*, is calculated using equation (11). The value for the internal resistance, R , can be adjusted by visually matching the modelled value P^* to the scatter data for $P_{measured}$, keeping the resulting line within the middle of the scatter plot in the area where it seems to broadly keep in a line (albeit a gently bended one), before it starts levelling off at low load.

Next, the Faraday's efficiency from measured data was estimated by using equation (13). At this point, after calculating U_{stack} from Equation (4), we can plot a scatter of $\eta_{F,est}$ as a function of or each experimental data point. This scatter plot is shown in Figure 1, which follows the expected Faradaic efficiency curve from literatures well [59]. It is noticeable that some of the values for $\eta_{F,est}$ are above 1, which is a physical impossibility (except perhaps at transient states), however this is caused by the scatter in the experimental data around which the model is built (the model will underestimate some values of power consumption as a consequence of driving the modelled curve for $P_{measured}$ vs. n_{H2} through the middle of the scatter plot for the experimental data).

On Figure 1, the curve obtained from the modelled Faradaic efficiency using equation (16) was adjusted to fit through the scatter plot for $\eta_{F,est}$. On Figure 1, the activation potential ΔU_{act} determined the rise of the curve from 0 shortly after the reversible potential. The constants x_1 and x_2 determined the slope and the position of the middle section that rises steeply between values near 0 and values near 1 for the Faradaic efficiency. Therefore these three constants were first adjusted for a good visual match of the model to the scatter in Figure 1, and then fine-tuned in the main model graph for P_{model} vs. n_{H2}, Figure 2, in an iterative process that adjusted these three parameters in turn with the electrode resistance R from equation (10) for the full model. The resistance was found to be a sensitive parameter, so once a suitable value was established, majority of the fine-tuning was done by the other parameters.

With the parameters from equation (16) settled, the power to hydrogen curve in Figure 2 was finalised. For the electrolyser H45, the adjustable parameters are listed in Table 1. The power conversion factor is an important link between the hydrogen produced and the power measured.

The model was tested against data taken every minute from BGH's 250 kW PEM electrolyser, known as H45, and the finished model is seen in Figure 2. Due to the limited available data, the model with its chosen parameters was created using data taken every minute for one 24-hour period, and then tested against two other sets of 1-minute data during two 24 hour periods. The day chosen for developing the model had most activity from the electrolyser, and therefore had more available data points. The effect of including the changing Faraday's efficiency defined by equation (16) is seen by comparing the curve of the model to an assumed Faraday's efficiency of 1.

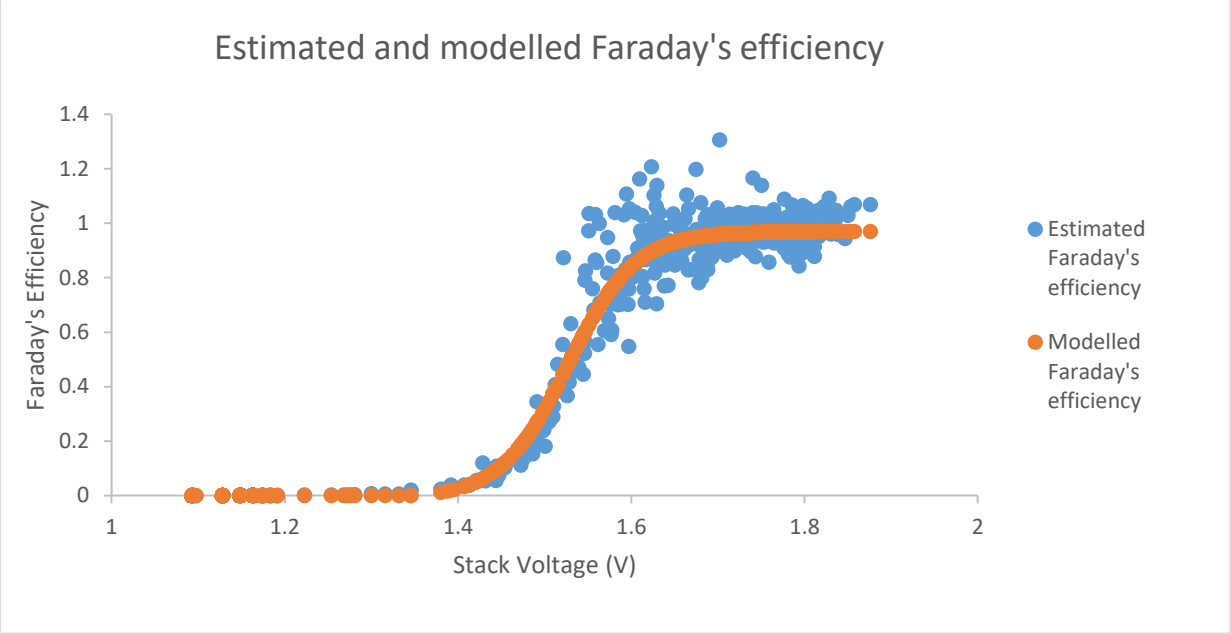

Figure 1. Faraday's efficiency curve fitting, measured data and modelled data

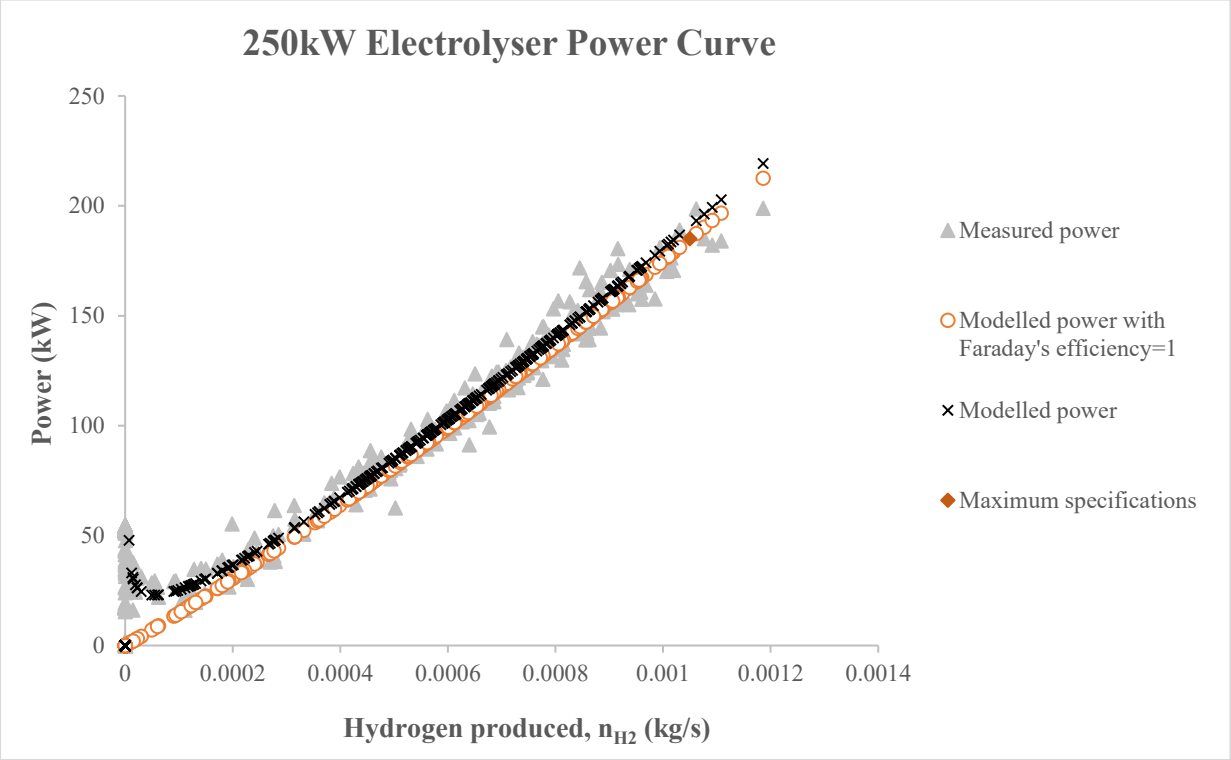

Figure 2. Power to the stack vs rate of production, for the model fitted against measured data (June 1st, 2017) from Bright Green Hydrogen's 250 kW PEM electrolyser. The curve 'Modelled Power' includes the equation for Faraday's efficiency from Figure 1.

Table 1 BGH 250 kW electrolyser model parameters

Symbol	Description	Value	Unit
η_{conv}	Power conversion factor	0.74	
R	Electrolyte resistance	$2*10^{-6}$	Ohms
ΔU_{act}	Overpotential	0.12	V
x_1	$x_1 = \frac{\left(\frac{zF}{0.5 * R_{gas}T}\right)}{A}$	$A = 6$	
x_2	Constant including effect of exchange current	70	V^{-1}

2.4 Comparing our Model to the 'Linear Model'

Section 1.3 mentioned that for commercial electrolysers, the voltage is often expressed as a linear function in relation to the current [38]. Due to the linear variation of voltage and current, this model is referred to as the 'Linear Model' in this paper, nevertheless the equations involved still result in a non-linear relationship between power and hydrogen production. In this model, the voltage is defined as [46]:

$$U = e_{min} + I_{H2} R_{lin} \quad (17)$$

where e_{min} is the minimum potential above which hydrogen production becomes significant (including electrode overpotentials, and in the range of validity of the Tafel law), and R_{lin} is the internal resistance as approximated in this model.

The voltage can then be found at different currents from Equation (17), where the current I_{H2} is obtained from Equation (6). The assumption can also be made that the Faradaic efficiency is 1, i.e. $I = I_{H2}$.

The resulting model for the power input to the stack is obtained by multiplying Equation (17) by I. Please note that this model produces a curve for P vs. n_{H2} that has the shape of a segment of parabola.

The value for e_{min} in this model can be assumed to be 1.48 V as in [28] or slightly higher to accommodate electrode overpotentials. Figure 3 shows that for the electrolyser, the value of R_{lin} that fitted well with the data on the near linear part at sufficiently high load was found to be $4 \cdot 10^{-6}$ Ohms. No further adjustment was made other than this visual fit.

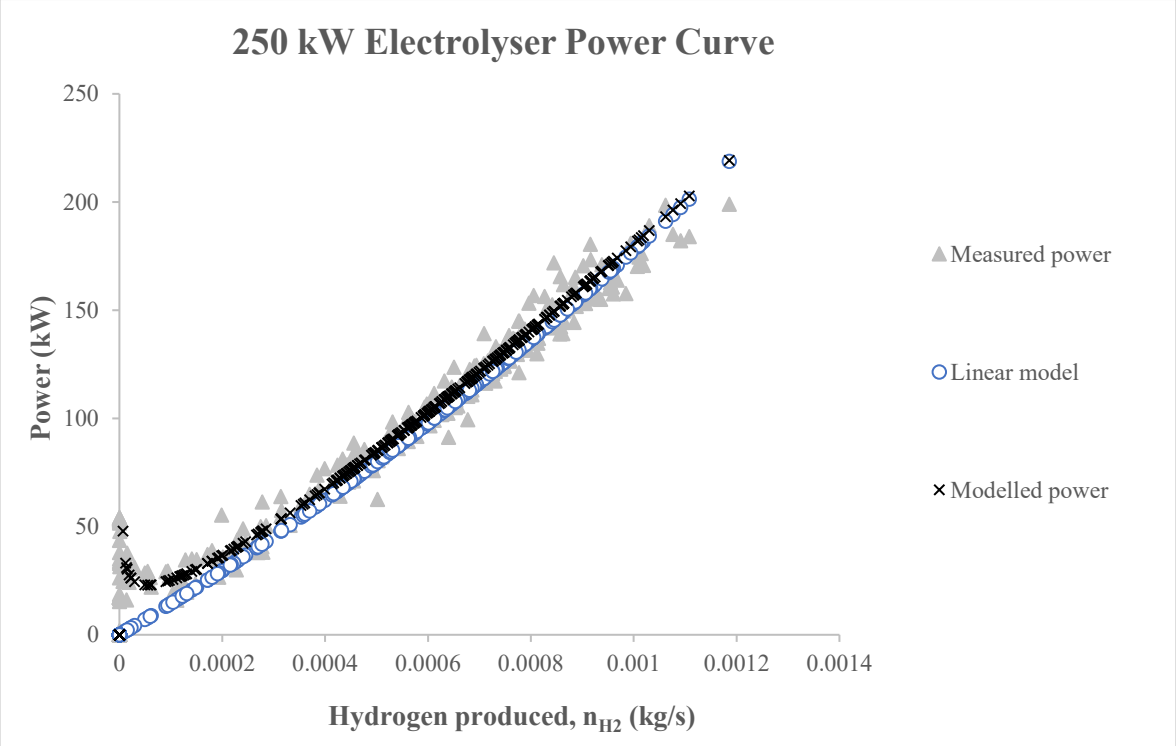

Figure 3. 'Linear Model' fitted to measured data (Power to the stack vs rate of production) from the H45 250 kW electrolyser (June 1st, 2017, same set as for Figs. 1 and 2), also compared with full model

3 Results

3.1 Data Validation

As mentioned in section 2.3, the model parameters were adjusted using 1 minute-interval data from a 24 hour period from 1st of June 2017 as the chosen electrolyser had a lot of activity from this day and therefore had a good number of data points. Two other sets were chosen to validate the model and its parameters. These results can be seen in Figure 4 and Figure 5. The model was able to follow the two data sets well. All three graphs show that the measured data first curves downwards as hydrogen output increases from 0, before bottoming-out and then nearly linearly increasing its power usage as hydrogen output increases. This was unexpected, although the model that we developed was still able to follow this pattern well at all three dates. The Linear Model has been included as a comparison.

Grouping all data points from Figure 3, Figure 4 and Figure 5 gives a more complete picture of the range of measured data from the electrolyser. This has been summarised Figure 6.

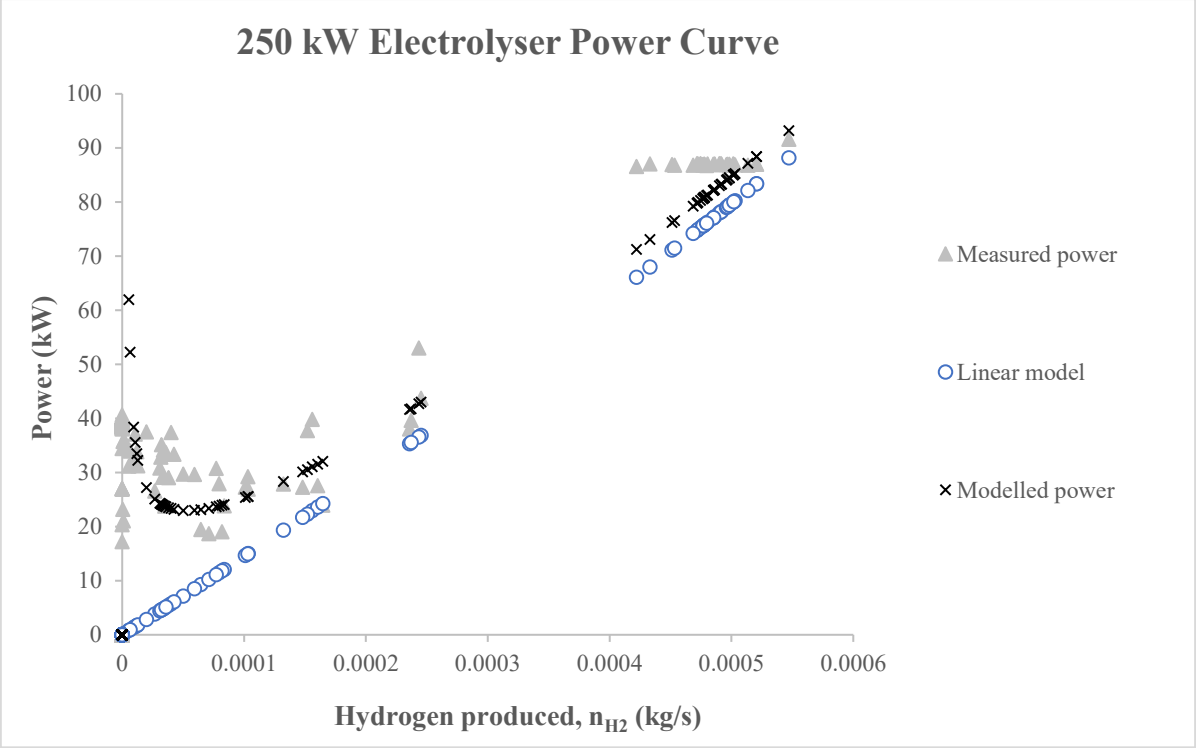

Figure 4. Model validation against measured data, Example 1 (May 30th, 2017) from Bright Green Hydrogen's 250 kW PEM electrolyser

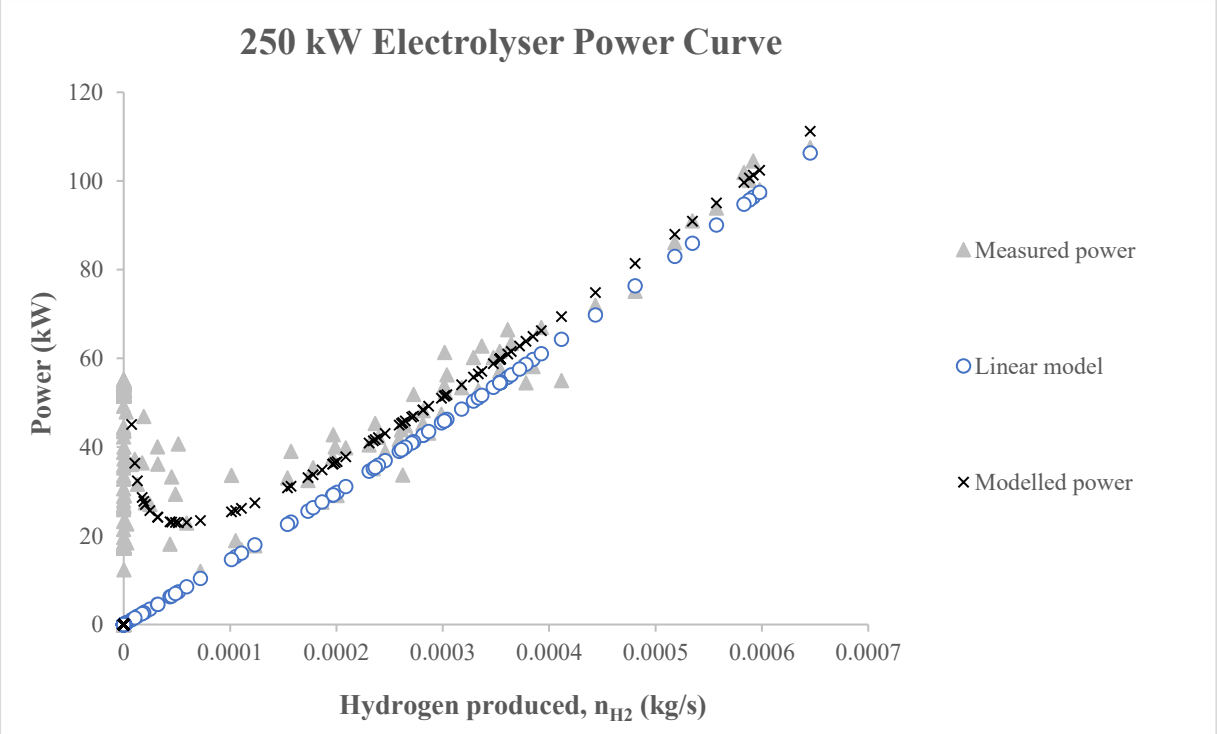

Figure 5. Model validation against measured data, Example 2 (June 2nd, 2017) from Bright Green Hydrogen's 250 kW PEM electrolyser

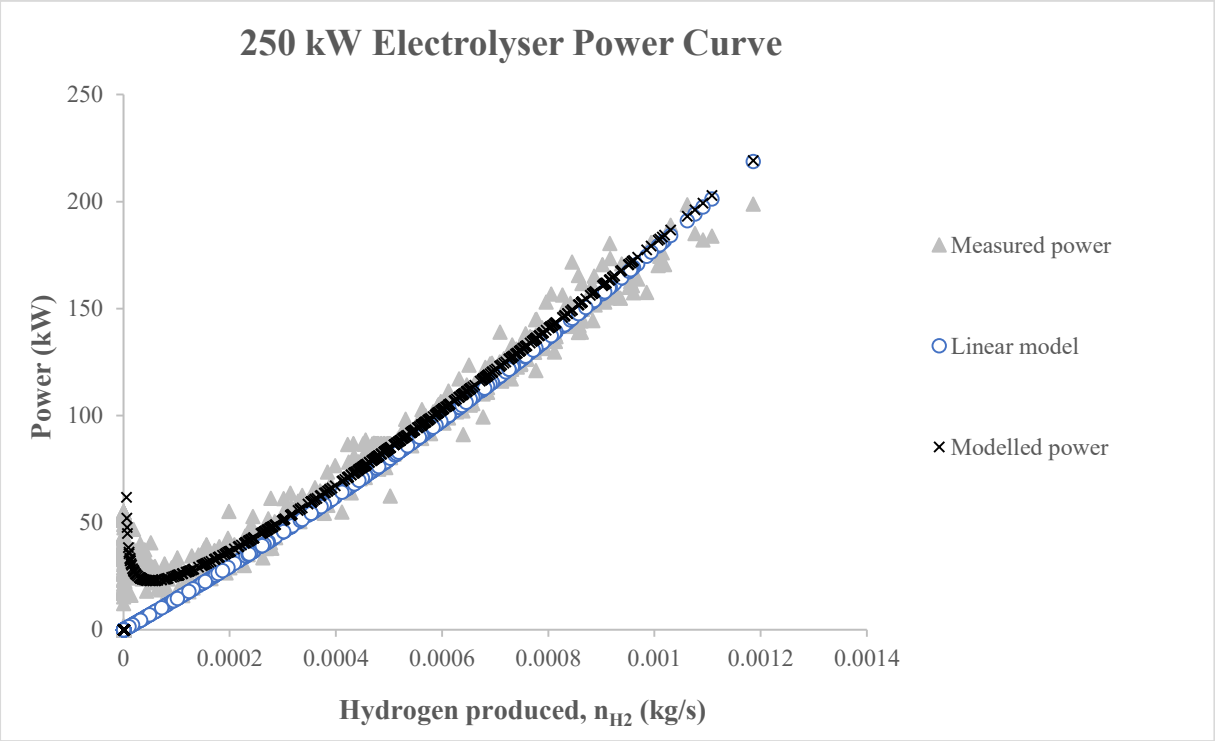

Figure 6. All data points from Figures 3, 4 and 5 summarised

4 Discussion

The developed electrolyser model allowed improved prediction of hydrogen output at low load. It also allowed more realistic transitions between periods when the electrolyser is idle (when energy consumption is dominated by parasitic stand-by loads) and periods when the electrolyser is producing hydrogen at low load. Better modelling of these two aspects become particularly relevant when estimating the economic performance as well as dynamic behaviour of the wider system including power consumption and hydrogen production.

All the data presented here are for the electrolyser at hot standby, which is one possible explanation as to why the power is observed to start in the range of 40 kW to 60 kW and decreases first with the increasing hydrogen production before it curves up again. This feature is also compatible with our proposed model as discussed below.

The region of high hydrogen production in Figure 4 appears to have a constant power consumption at around 87 kW with a varying hydrogen output ranging from 0.43 g/s to 0.54 g/s. Closer inspection of the underlying minute-by-minute data shows that the full range of this variation occurred within 2 minutes, followed by fluctuations within this range. This strongly suggest pressure-driven oscillations of the flow. This suggestion is further supported by an analysis of the data in the run-up to this event: in the previous 45 minutes, the power consumption by the stack varied in the range 82 – 143 kW, corresponding to an estimated production of about 1.7 kg of hydrogen, and yet no hydrogen flowed from the stack. It is likely that this power is used for pressurising (and possibly flushing or even heating up) the stack, its casing and surrounding pipework. The build-up of gas within the electrolyser prior to operating pressure being reached would probably explain some of the scatter that is observed in the raw data that we are presenting here. Our model (and standard industry models such as the 'Linear Model') may account well for average values, but miss out on transient phenomena such as this. However, over longer timescales the fluctuations may average out with the result that predictions from models may remain relatively close to time-averaged observed values. It is important to highlight that 1-minute data will show more variations like this, than half-hourly or hourly data, suggesting perhaps that depending on the final use of a model, too fine a time-resolution for the data may or may not be a desirable requirement. Meanwhile, using hourly data for energy systems modelling can be too general depending on the analysis carried out from the data.

4.1 Performance comparison between the models

The 'Linear Model' used in comparison for commercial electrolyser modelling successfully captured a major part of the electrolyser's behaviour through a straightforward calculation. Its limitation was in simulating the lower hydrogen production flow rates. This is shown in Figure 3, which has already been used to illustrate the adjustment of the value of R_{lin} in the 'Linear Model'. It can be seen that this method works well for the majority of the power curve, however the inaccuracy of the common model becomes noticeable at hydrogen production levels below about 30% of the nominal rate of hydrogen production (ca. 0.3 g/s).

By contrast, our new model is particularly suited to match the same pattern, simply because it accounts for low Faraday efficiency when the load is becoming low. This feature allows it to reach a minimum power consumption at some point in the low range of hydrogen production, before increasing again as energy efficiency losses increase with increased hydrogen production.

The impact of this difference on performance is summarised in

Table 2, where it appears that increased accuracy at lower load allows our new model to make a closer prediction to the actual energy consumption.

This work shows the impact of Faraday's efficiency at low load, thus improving the prediction of hydrogen production and energy consumption for a relatively simple model of a commercial electrolyser. In Figure 3 the 'Linear model' has nearly an 8% error while this model has around 3% error. Figure 4 mostly has lower hydrogen flow rates, resulting in a greater difference between the predicted energy consumption and the actual energy consumption. The 'Linear model' is off by 43% and this paper's model is off by 25%. In Figure 5's example, the linear model's energy consumption is off by 30% and this model is off by 16%.

Table 2. Actual energy consumed by the electrolyser stack when it is producing hydrogen over 24 hour period compared to modelled energy consumed (data from hot standby and pressurisation is excluded)

Figure	Actual energy consumed by stack over 24 hr (kWh)	New model's prediction of energy consumed over 24 hr (kWh)	% error for new model	Linear model's prediction of energy consumed over 24 hr (kWh)	% error for linear model
3	565	549	– 2.8	519	– 8.1
4	87	65	– 25	50	– 43
5	82	69	– 16	57	– 30

Table 3. Losses from hot stand-by (excluding pressurization).

Figure	Actual energy consumed by stack over 24 hr, excluding hot standby (kWh)	Actual energy consumed by stack over 24 hr, including hot standby (kWh)	% of total energy consumed by stack while on hot standby	Actual average hot standby power (kW)
3	565	1210	53	44 ± 15.3 (standard deviation)
4	87	235	63	38 ± 4.8 (standard deviation)
5	82	1064	92	45 ± 14.9 (standard deviation)

4.2 Hot standby losses

It is important to highlight the impact of the parasitic load of the electrolyser when it is on 'hot standby', i.e. kept under low power and heated so that it can start generating hydrogen at very short notice. In principle, this parasitic load could result in a major energy consumption without a hydrogen output.

The plant data showed that this particular electrolyser used roughly 38 – 45kW in parasitic load for the electrolyser alone when it was on hot standby, as shown in Table 3. After factoring in the conversion losses, this represented 25% of the full 250 kW power. This figure seems high, especially when comparing to other published standby losses of a protective current of 0.35 kW for a 25 kW alkaline electrolyser [36] (representing 1.4% of full capacity) or 7 kW at hibernation (25 kW when including freezing protection) for a 2 MW electrolyser machine [60] (0.35% or 1.25% of full capacity). However, it may be appropriate to point out that this particular electrolyser was built based on a pre-existing 500 kW electrolyser model, and therefore there is a possibility that it might not be as efficient at hot standby as an optimised, commercial 250 kW electrolyser should be.

In addition to this, operation on standby or at low load will require the application of low power, and unless the power supply unit is specially designed or adapted to retain high efficiency at low load it may well be the source of significant heating and power draw. Thus, rectifiers for which typical efficiencies are 88-91% (see for example [61]) are known to use significantly more power at lower load especially if based on traditional thyristor technology. For example, in [62] it is shown that a 6-pulse thyristor rectifier operated at a partial load of 20% for an electrolyser can increase overall power consumption by up to 20% compared with what would be expected if its efficiency at full load was constant (i.e. the equivalent of applying $\frac{\eta_{conv}}{1.2} = 0.62$ instead of 0.74, or an additional load of 12% of 50 kW = 6 kW), whereas a buck rectifier can maintain the same performance over this range. Likewise, [63] investigated two common configurations of DC power supply to electrolysers and their results suggested losses of energy efficiency of the order of 3-4 percentage points (in terms of HHV of hydrogen over electrical energy) when going from 100% load to 20% load, with one power system also being 3-4 percentage points more efficient than the other over the entire range of loads. It is possible that in the particular case of the LCEP the power supply unit may have needed further consideration regarding its efficient operation at low load and at hot stand-by.

With the standby power representing such a significant proportion of the nominal power of the electrolyser, long periods of standby will result in large energy penalties, and this was in fact observed. Table 3 also presents the data on energy consumption during hot standby for all three days that the data was gathered for this work. The % of energy that was consumed by the stack operation during hot standby periods ranged from 53 to 92 % of the total energy sent to the stack (we discounted energy consumption from the pressurisation of the stack). These high figures highlight the issue with just modelling the electrolyser as an isolated component and not as a system that is ready to produce hydrogen when needed. This also suggests a very inefficient specification or operation of the control system, where perhaps the algorithm is not following an optimised process when deciding to maintain the electrolyser on hot standby or switch it on. This proves the importance of a carefully planned control scheme of an electrolyser, where a combination of forecast available power and analysis of actual available power (ensuring there is a sustained power input), could reduce the hot standby time and therefore improve the electrolyser's performance.

Future work should therefore focus on optimising the control scheme so that unnecessary standby operation is avoided. This will be investigated further for a study on whole LCEP system where this electrolyser model is a part of, to improve the LCEP control scheme.

5. Conclusion

An electrolyser model has been developed using real-world data from a commercial electrolyser using limited available information. The model is semi-empirical and the key data needed is the power usage and the hydrogen produced by the electrolyser. From this, certain parameters can be adjusted to fit the model to the available data of a specific electrolyser and then use the modified model to realistically capture the commercial electrolyser's

power input and hydrogen output. This makes this model useful for whole system modelling for future planning and optimisation, where it is important to capture the actual behaviour but not over-complicating the model as this would sacrifice simulation time efficiency.

The model also incorporated an original semi-empirical approach to estimate Faradaic efficiency from plant data.

The model can be applied to other commercial electrolysers by readjusting the parameters. It can be adapted to different operating temperatures and pressure since parameters of the model can themselves be described as functions of temperatures and pressure, as can also be done for other models. Furthermore the equations can be adapted and calculated in a different order so that a user with for example just power and current data can use this model too, as we know is the case at another demonstration site.

The model was first developed using one set of data to determine the adjustable parameters, and then validated against other collections of data for the same electrolyser. The model was able to successfully capture the pattern seen in the validation data, in particular the transition between standby mode and operation at low load, and the minimum point of power consumption that is observed as hydrogen output increases from 0.

A comparison was made between this model and a commonly used model in industry, referred to here as the 'Linear Model' to see if there was an improvement in capturing the power consumption more accurately at lower hydrogen outputs. This was found to be the case, and our model was found to perform significantly better than the common one, especially on days when production was relatively low. It also would be more easily combined with system models where standby power consumption is included, allowing for a smoother transition for the modelling of the power supply between standby and production at low load.

The model offers an alternative for users of commercial electrolysers whose systems may be affected by low capacity of utilization at times, for example due to daily, weekly or seasonal patterns of power supply or demand, as can be expected in many contexts where renewable energies or remote locations are involved.

As an important aside, the particular electrolyser to which our model was applied in this study had roughly 25% parasitic load when it was on hot standby. Looking at the whole system that was part of LCEP, it became apparent that the control system needed optimised, because the long periods of time over which the electrolyser was on hot standby resulted in excessive cumulated energy consumption of the same order as that observed during production. While it may be technically difficult to avoid power consumption during stand-by, it should be able to be minimised. Additionally improvements in the control system have the potential to vastly increase the energy efficiency of the electrolyser, by more judiciously choosing to switch between hot or cold standby (or even temporary shutdown). This could be done on the basis of real time forecast of power supply, power demand and current inventory of stored hydrogen. Finally, it is possible that the power supply unit including the rectifier may need to be reviewed regarding its efficiency at low load and at hot stand-by, as in a worst case scenario it could account for much of the observed parasitic load.

Other interesting observations made in the course of this project were that

- Dynamic changes in the recorded flow rate of produced hydrogen was apparent in the minute-by-minute data which were used in this paper
- These transient changes could explain some of the scatter in the data (in one case, 21% variation in two minutes)
- Some of these transient changes in the flow rate may have been driven by fluctuations in pressure caused by the control valve that regulates the internal pressure of the electrolyser stack
- Some amount of time and energy seemed to be expended to provide the cushion hydrogen gas that is required for bringing the electrolyser to its operating pressure (up to 45 minutes in one case). During these periods, no hydrogen seemed to be produced.
- Transient phenomena could be captured by the minute-to-minute data, but our model and the standard 'linear' model would ignore these and average over time to give values close to observed data over longer periods of time.

Acknowledgements:

The authors wish to thank Energy Technology Partnership, Bright Green Hydrogen and the School of Engineering at the University of Edinburgh for supporting this work through Maja Persson's PhD scholarship.

References

[1] R. Steinberger-Wilckens, J. Radcliffe, P. E. Dodds, A. Velazquez Abad, and Z. Kurban, "The role of hydrogen and fuel cells in delivering energy security for the UK," London, UK, 2017.
[2] I. Staffell and P. E. Dodds, "The role of hydrogen and fuel cells in future energy systems," London, UK, 2017.
[3] M. J. Smith, K. Turner, and J. T. S. Irvine, "The Economic Impact of Hydrogen and Fuel Cells in the UK – A Preliminary Assessment based on Analysis of the replacement of Refined Transport Fuels and Vehicles.," London, UK, 2017.
[4] European Commission, "A hydrogen strategy for a climate-neutral Europe," Brussels, 2020.
[5] Committe on Climate Change, "Net Zero: The UK's contribution to stopping global warming," *Committe Clim. Chang.*, no. May, p. 275, 2019.
[6] Scottish Government, "Energy Statistics Database," 2019. [Online]. Available: https://www2.gov.scot/Topics/Statistics/Browse/Business/Energy/Database. [Accessed: 29-Aug-2019].
[7] M. Joos and I. Staffell, "Short-term integration costs of variable renewable energy: Wind curtailment and balancing in Britain and Germany," *Renew. Sustain. Energy Rev.*, vol. 86, pp. 45–65, Apr. 2018.
[8] Scottish Enterprise, "Constrained Renewables and Green Hydrogen Production Study Final Report," 2018.
[9] N. Skopljak, "ScotWind Offshore Wind Leasing Round Kicks Off | Offshore Wind," 10-Jun-2020. [Online]. Available: https://www.offshorewind.biz/2020/06/10/scotwind-offshore-wind-leasing-round-kicks-off/. [Accessed: 10-Aug-2020].
[10] Scottish Government, *Draft Sectoral Marine Plan for Offshore Wind Energy (2019)*, no. December. Edinburgh, 2019.
[11] The Scottish Government, "Scottish Energy Strategy: The future of energy in Scotland," Edinburgh, 2017.
[12] BEIS, "The Clean Growth Strategy," London, 2017.
[13] Scottish Government, "Scottish greenhouse gas emissions 2017 - gov.scot," 2017. [Online]. Available: https://www.gov.scot/publications/scottish-greenhouse-gas-emissions-2017/pages/3/. [Accessed: 29-Aug-2019].
[14] C. A. Schug, "Operational Characteristics of High-Pressure, High-Efficiency Water-Hydrogen-Electrolysis," *Int. J Hydrog. Energy*, vol. 23, pp. 1113–1120, 1998.
[15] P. Hou, P. Enevoldsen, J. Eichman, W. Hu, M. Z. Jacobson, and Z. Chen, "Optimizing investments in coupled offshore wind -electrolytic hydrogen storage systems in Denmark," *J. Power Sources*, vol. 359, pp. 186–197, 2017.
[16] J. Samaniego, F. Alija, S. Sanz, C. Valmaseda, and F. Frechoso, "Economic and technical analysis of a hybrid wind fuel cell energy system," *Renew. Energy*, vol. 33, no. 5, pp. 839–845, 2008.
[17] California Hydrogen Business Council, "Power-to-Gas: The Case for Hydrogen White Paper," Los Angeles, 2015.
[18] P. Enevoldsen and B. K. Sovacool, "Integrating power systems for remote island energy supply: Lessons from Mykines, Faroe Islands," *Renew. Energy*, vol. 85, pp. 642–648, 2016.
[19] M. Santarelli, M. Call, and S. Macagno, "Design and analysis of stand-alone hydrogen energy systems with different renewable sources," *Int. J. Hydrogen Energy*, vol. 29, no. 15, pp. 1571–1586, 2004.
[20] A. Pfeifer, P. Prebeg, and N. Duić, "Challenges and opportunities of zero emission shipping in smart islands: A study of zero emission ferry lines," *eTransportation*, vol. 3, 2020.
[21] The European Marine Energy Centre Ltd, "Hydrogen Projects," *EMEC Hydrogen*, 2020. [Online]. Available: http://www.emec.org.uk/projects/hydrogen-projects/. [Accessed: 10-Aug-2020].
[22] Orkney Islands, "About — BIG HIT," 2019. [Online]. Available: https://www.bighit.eu/about. [Accessed: 30-Aug-2019].
[23] European Parliament, "POLITICAL DECLARATION on CLEAN ENERGY FOR EU ISLANDS," Valletta, May 2017.
[24] R. Gazey, S. K. Salman, and D. D. Aklil-D'Halluin, "A field application experience of integrating hydrogen technology with wind power in a remote island location," *J. Power Sources*, vol. 157, no. 2, pp. 841–847, 2006.
[25] M. Bielmann, U. F. Vogt, M. Zimmermann, and A. Züttel, "Seasonal energy storage system based on hydrogen for self sufficient living," *J. Power Sources*, vol. 196, no. 8, pp. 4054–4060, 2011.
[26] M. Reuß, T. Grube, M. Robinius, P. Preuster, P. Wasserscheid, and D. Stolten, "Seasonal storage and

alternative carriers: A flexible hydrogen supply chain model," *Appl. Energy*, vol. 200, pp. 290–302, 2017.
[27] A. Amid, D. Mignard, and M. Wilkinson, "Seasonal storage of hydrogen in a depleted natural gas reservoir," *Int. J. Hydrogen Energy*, vol. 41, no. 12, pp. 5549–5558, 2016.
[28] M. A. Pellow, C. J. M. Emmott, C. J. Barnhart, and S. M. Benson, "Hydrogen or batteries for grid storage? A net energy analysis," *Energy Environ. Sci.*, vol. 8, no. 7, pp. 1938–1952, 2015.
[29] S. Samsatli and N. J. Samsatli, "The role of renewable hydrogen and inter-seasonal storage in decarbonising heat – Comprehensive optimisation of future renewable energy value chains," *Appl. Energy*, vol. 233–234, no. June 2018, pp. 854–893, 2019.
[30] Aberdeen City Council, "H2 Aberdeen | About Hydrogen," 2019. [Online]. Available: http://www.h2aberdeen.com/home/H2-Aberdeen-about-hydrogen.aspx. [Accessed: 13-Feb-2019].
[31] Aberdeen City Council, "Aberdeen hydrogen re-fuelling station opens to the public," *Aberdeen City Council*, 2018. [Online]. Available: https://news.aberdeencity.gov.uk/aberdeen-hydrogen-re-fuelling-station-opens-to-the-public/. [Accessed: 13-Feb-2019].
[32] Orkney Islands, "Orkney Hydrogen | Surf 'n' Turf," 2019. [Online]. Available: http://www.surfnturf.org.uk/. [Accessed: 30-Aug-2019].
[33] H. Norman and A. C. Market, "Hydrogen Office opens in Scotland," *Fuel Cells Bull.*, vol. 2011, no. 2, pp. 9–10, 2011.
[34] L. Valverde-isorna, D. Ali, and D. Ali, "A technical evaluation of Wind-Hydrogen (WH) demonstration projects in Europe A technical eval luation of Wind-Hyd drogen (WH) demonstr ration projects in Eur rope on," no. May, 2013.
[35] A. H. A. Rahim, A. S. Tijani, S. K. Kamarudin, and S. Hanapi, "An overview of polymer electrolyte membrane electrolyzer for hydrogen production: Modeling and mass transport," *J. Power Sources*, vol. 309, pp. 56–65, 2016.
[36] A. Buttler and H. Spliethoff, "Current status of water electrolysis for energy storage, grid balancing and sector coupling via power-to-gas and power-to-liquids: A review," *Renew. Sustain. Energy Rev.*, vol. 82, no. February 2017, pp. 2440–2454, 2018.
[37] A. Ursúa and P. Sanchis, "Static-dynamic modelling of the electrical behaviour of a commercial advanced alkaline water electrolyser," *Int. J. Hydrogen Energy*, vol. 37, no. 24, pp. 18598–18614, 2012.
[38] R. Sarrias-Mena, L. M. Fernández-Ramírez, C. A. García-Vázquez, and F. Jurado, "Electrolyzer models for hydrogen production from wind energy systems," *Int. J. Hydrogen Energy*, vol. 40, no. 7, pp. 2927–2938, 2015.
[39] Z. Abdin, C. J. Webb, and E. M. Gray, "Modelling and simulation of a proton exchange membrane (PEM) electrolyser cell," *Int. J. Hydrogen Energy*, vol. 40, no. 39, pp. 13243–13257, 2015.
[40] M. Shen, N. Bennett, Y. Ding, and K. Scott, "A concise model for evaluating water electrolysis," *Int. J. Hydrogen Energy*, vol. 36, no. 22, pp. 14335–14341, 2011.
[41] H. Görgün, "Dynamic modelling of a proton exchange membrane (PEM) electrolyzer," *Int. J. Hydrogen Energy*, vol. 31, no. 1, pp. 29–38, 2006.
[42] F. Z. Aouali *et al.*, "Modelling and experimental analysis of a PEM electrolyser powered by a solar photovoltaic panel," *Energy Procedia*, vol. 62, pp. 714–722, 2014.
[43] A. S. Tijani, N. A. B. Yusup, and A. H. A. Rahim, "Mathematical Modelling and Simulation Analysis of Advanced Alkaline Electrolyzer System for Hydrogen Production," *Procedia Technol.*, vol. 15, pp. 798–806, 2014.
[44] P. Olivier, C. Bourasseau, and B. Bouamama, "Modelling, simulation and analysis of a PEM electrolysis system," *IFAC-PapersOnLine*, vol. 49, no. 12, pp. 1014–1019, 2016.
[45] M. Hammoudi, C. Henao, K. Agbossou, Y. Dubé, and M. L. Doumbia, "New multi-physics approach for modelling and design of alkaline electrolyzers," *Int. J. Hydrogen Energy*, vol. 37, no. 19, pp. 13895–13913, 2012.
[46] O. Atlam and M. Kolhe, "Equivalent electrical model for a proton exchange membrane (PEM) electrolyser," *Energy Convers. Manag.*, vol. 52, no. 8–9, pp. 2952–2957, 2011.
[47] R. García-Valverde, N. Espinosa, and A. Urbina, "Simple PEM water electrolyser model and experimental validation," *Int. J. Hydrogen Energy*, vol. 37, no. 2, pp. 1927–1938, 2012.
[48] A. Awasthi, K. Scott, and S. Basu, "Dynamic modeling and simulation of a proton exchange membrane electrolyzer for hydrogen production," *Int. J. Hydrogen Energy*, vol. 36, pp. 14779–14786, 2011.
[49] P. Olivier, C. Bourasseau, and B. Bouamama, "Dynamic and multiphysic PEM electrolysis system modelling: A bond graph approach," *Int. J. Hydrogen Energy*, vol. 42, no. 22, pp. 14872–14904, 2017.
[50] T. Zhou and B. Francois, "Modeling and control design of hydrogen production process for an active hydrogen/wind hybrid power system," *Int. J. Hydrogen Energy*, vol. 34, no. 1, pp. 21–30, 2009.
[51] Ø. Ulleberg, "Modeling of advanced alkaline electrolyzers:a system simulation approach," *Int. J. Hydrogen Energy*, vol. 28, pp. 21–33, 2003.

[52] E. Zoulias, E. Varkaraki, and N. Lymberopoulos, “A review on water electrolysis,” *Centre of Renewable Energy Source, Frederick Research Centre*. [Online]. Available: http://large.stanford.edu/courses/2012/ph240/jorna1/docs/zoulias.pdf. [Accessed: 28-Nov-2018].
[53] F. J. Pino, L. Valverde, and F. Rosa, “Influence of wind turbine power curve and electrolyzer operating temperature on hydrogen production in wind-hydrogen systems,” *J. Power Sources*, vol. 196, no. 9, pp. 4418–4426, 2011.
[54] T. Yigit and O. F. Selamet, “Mathematical modeling and dynamic Simulink simulation of high-pressure PEM electrolyzer system,” *Int. J. Hydrogen Energy*, vol. 41, pp. 13901–13914, 2016.
[55] D. Pletcher and F. Walsh, *Industrial Electrochemistry*, 2nd Ed. London: Blackie Academic & Professional, 1990.
[56] J. O. Jensen, S. Hojgaard Jensen, and N. Tophoj, “Pre-investigation of water electrolysers,” 2008.
[57] P. H. Rieger, *Electrochemistry*, 2nd ed. Springer Science + Business Media Dordrecht, 1994.
[58] A. Robertson, “Levenmouth Community Energy Project Hydrogen Microgrid Electrical Simulation Model,” University of Glasgow, 2018.
[59] A. Khalilnejad, A. Sundararajan, and A. I. Sarwat, “Optimal design of hybrid wind/photovoltaic electrolyzer for maximum hydrogen production using imperialist competitive algorithm,” *J. Mod. Power Syst. Clean Energy*, vol. 6, no. 1, pp. 40–49, 2018.
[60] K. Hyde and A. Ellis, “Feasibility of Hydrogen Bunkering,” Jan. 2019.
[61] L. LINYI SOURCE RECTIFIER CO, “Electrolysis rectifier.” [Online]. Available: http://www.igbtrectifier.com/electrolysis rectifier.html. [Accessed: 13-Aug-2020].
[62] J. Koponen, V. Ruuskanen, A. Kosonen, M. Niemela, and J. Ahola, “Effect of Converter Topology on the Specific Energy Consumption of Alkaline Water Electrolyzers,” *IEEE Trans. Power Electron.*, vol. 34, no. 7, pp. 6171–6182, Jul. 2018.
[63] A. Ursúa, P. Sanchis, and L. Marroyo, *Renewable Hydrogen Technologies Production, Purification, Storage, Applications and Safety*, First Edit. Elsevier Science, 2013.